Bioactive Materials 35 (2024) 31–44

Contents lists available at ScienceDirect

Bioactive Materials

journal homepage: www.keaipublishing.com/en/journals/bioactive-materials

Highly active probiotic hydrogels matrixed on bacterial EPS accelerate wound healing via maintaining stable skin microbiota and reducing inflammation

Hongtao Xu [a], Yaqian Li [a], Jiangping Song [a], Liuyang Zhou [a], Kaizhang Wu [a], Xingyu Lu [a], XiaoNing Zhai [a], Zhili Wan [b,**], Jie Gao [a,*]

[a] School of Light Industry and Food Engineering, Guangxi University, Nanning, 530004, China
[b] Laboratory of Food Proteins and Colloids, School of Food Science and Engineering, South China University of Technology, Guangzhou, 510640, China

ARTICLE INFO

Keywords:
Wound healing
Probiotics hydrogel
Skin microbiota
Lactobacillus paracasei
Extracellular polysaccharides

ABSTRACT

Skin microbiota plays an important role in wound healing, but skin injuries are highly susceptible to wound infections, leading to disruption of the skin microbiota. However, conventional antibacterial hydrogels eliminate both probiotics and pathogenic bacteria, disrupting the balance of the skin microbiota. Therefore, it is important to develop a wound dressing that can fend off foreign pathogenic bacteria while preserving skin microbiota stability. Inspired by live bacteria therapy, we designed a probiotic hydrogel (HAEPS@*L.sei* gel) with high viability for promoting wound healing. *Lactobacillus paracasei TYM202* encapsulated in the hydrogel has the activity of promoting wound healing, and the hydrogel matrix EPS-M76 has the prebiotic activity that promotes the proliferation and metabolism of *Lactobacillus paracasei TYM202*. During the wound healing process, HAEPS@*L.sei* gel releases lactic acid and acetic acid to resist the growth of pathogenic bacteria while maintaining *Firmicutes* and *Proteobacteria* balance at the phylum level, thus preserving skin microbiota stability. Our results showed that live probiotic hydrogels reduce the incidence of inflammation during wound healing while promoting angiogenesis and increasing collagen deposition. This study provides new ideas for developing wound dressings predicated on live bacterial hydrogels.

1. Introduction

The skin is inhabited by millions of bacteria, archaea, fungi, and viruses, which are collectively known as the skin microbiota [1]. Similar to gut microbiota, skin microbiota play an important role in protecting the host from invading pathogens and regulating the immune system [2]. Some microorganisms colonized in the skin can act as a physical barrier against pathogen invasion [3,4]. Once the skin is damaged, harmful bacteria take the opportunity to invade the tissue and disrupt the balance of the skin's microbial system, resulting in tissue damage and wound infection [5]. This inevitably disrupts the wound-healing process, imposing significant challenges on patients and healthcare providers. To tackle this issue, researchers have developed diverse antibacterial hydrogels to expedite the healing of infected wounds [6]. These antibacterial hydrogels show great benefit in removing wound pathogens, but they inevitably inhibit the growth of probiotics in the skin, thus disrupting the skin microbiome [7]. Therefore, it is imperative to develop a wound dressing capable of repelling foreign pathogenic bacteria and preserving the stability of the skin microbiota, thereby reducing the incidence of infected wounds at the source.

Over the years, probiotic hydrogels have received much attention as a new intervention in the field of treatment of skin diseases [8]. They significantly improve the antimicrobial properties of hydrogels by producing antibacterial peptides or other metabolites from introduced live microbiota, avoiding the disadvantages of traditional antibacterial hydrogels [9]. Hydrogels encapsulating *Lactobacillus* can inhibit the growth of pathogenic bacteria by producing organic acids (lactic, acetic, formic, and malic) as well as other antimicrobial substances, have been shown to be an effective therapeutic option for wound healing [10–12]. Nevertheless, the risk of systemic infections and how to effectively

Peer review under responsibility of KeAi Communications Co., Ltd.
* Corresponding authors.
** Corresponding author.
E-mail addresses: zhiliwan@scut.edu.cn (Z. Wan), gaojie@gxu.edu.cn (J. Gao).

https://doi.org/10.1016/j.bioactmat.2024.01.011
Received 17 August 2023; Received in revised form 13 December 2023; Accepted 12 January 2024

maintain bacterial activity under complex external conditions have emerged as key challenges limiting the practical application of live bacterial therapy [13]. Recently, materials such as polysaccharides (chitosan, pectin, sodium alginate), proteins (gelatin and whey proteins) have been used to prepare hydrogels to deliver probiotics due to their excellent biocompatibility [14–16]. However, current protocols primarily concentrate on shielding probiotics from intricate external conditions but lack effectiveness in fostering probiotic proliferation and metabolism. Consequently, there is a necessity to find novel alternative materials that can enhance the physiological functions of encapsulated probiotics encapsulated in hydrogels.

Extracellular polysaccharides (EPS) are long-chain polysaccharide secreted by microorganisms during their growth and metabolism. These compounds play a pivotal role in enhancing the survival rate of microorganisms under external environmental pressures and are indispensable for probiotic functionality [17,18]. Moreover, functioning as a prebiotic, EPS has been shown to stimulate the proliferation and metabolic activity of probiotics [19]. Being a polysaccharide derived from microbial fermentation broth, EPS possesses qualities such as easy preparation, low cost, high yield, affinity for probiotics, eco-friendliness, and biodegradability [20,21]. Its abundant hydroxyl, carboxyl, and amino content renders it an outstanding material for hydrogel preparation [22]. Consequently, employing EPS for crafting live probiotic hydrogels emerges as a viable and feasible option.

In this study, we found a probiotic strain of *L. paracasei TYM*202 that can efficiently accelerate wound healing, and the EPS from *B. velezensis M76T11B* (EPS-M76) could promote the proliferation of *L. paracasei TYM202* and its production of acetic acid, lactic acid, and acetic acid. Next, we used the EPS-M76 as the probiotic-preferred matrix to encapsulate *L. paracasei TYM202* and create a live probiotic hydrogel. To achieve a robust probiotic hydrogel, we first modified EPS-M76 with dopamine to obtain an adhesion-enhanced EPS-M76 (DAEPS), then further introduced hyaluronic acid methacrylate (HAMA) into the DAEPS matrix. DAEPS and HAMA were utilized to form the initial cross-linking network through hydrogen bonding, and this was followed by a secondary cross-linking network through covalent cross-linking under light-induced conditions, resulting in the formation of HAMA-enhanced DAEPS multi-crosslinked probiotic hydrogel (Scheme 1). The probiotics encapsulated in the hydrogel are energetic and do not escape to the external environment. This live probiotic hydrogel has good mechanical properties and injectability, and its excellent biocompatibility demonstrates its great potential in clinical applications. Our results showed that this probiotic hydrogel was able to accelerate wound healing by reducing inflammation during the inflammatory phase, promoting the expression of vascular endothelial growth factor-α (VEGF-α) during the proliferative phase, and promoting collagen deposition during the

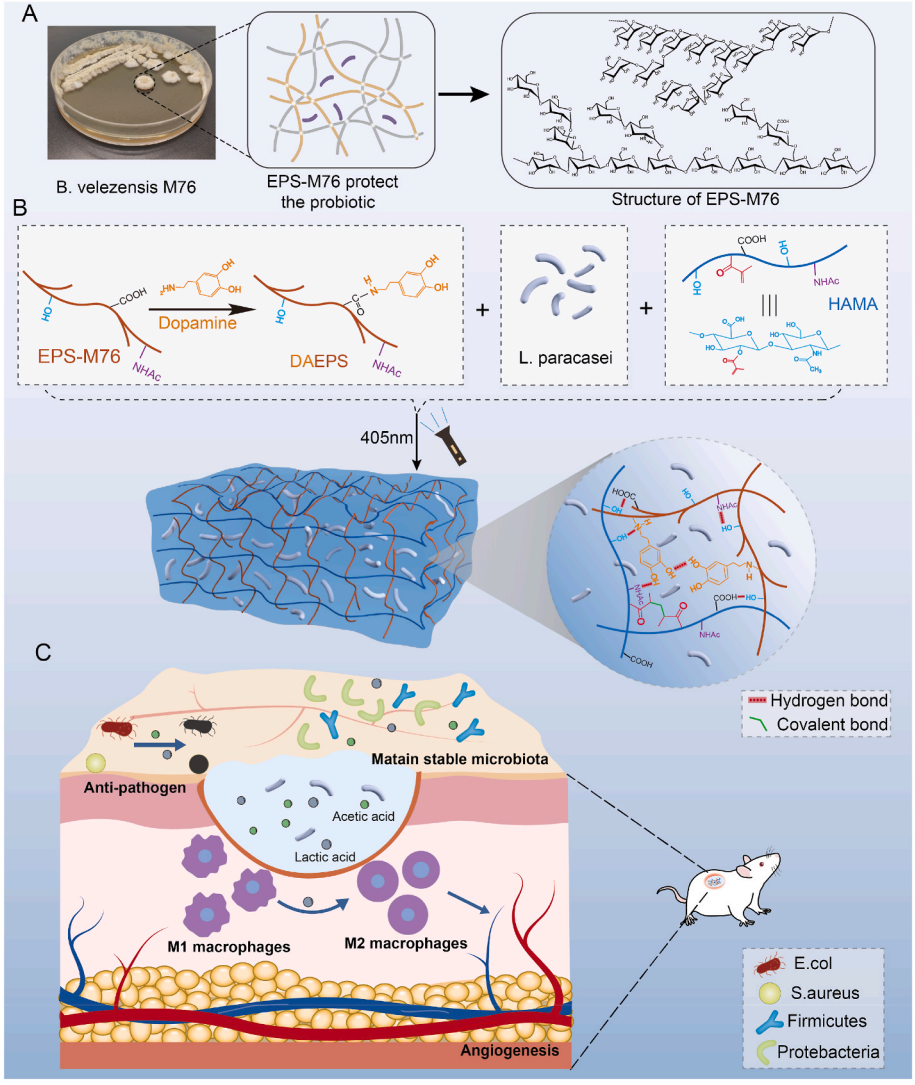

Scheme 1. (A) Structure of EPS-M76 with the probiotic protective effect. (B)Schematic illustration of the preparation of probiotic hydrogel (HAEPS@*L.sei* gel). (C) The biological mechanism under the wound healing capacity of HAEPS@L.sei gel.

remodeling phase. Notably, probiotic hydrogel kills skin pathogenic bacteria while maintaining the homeostasis of the skin microbiome, which provides a good physiological environment for various skin microorganisms and cells to perform their functions. This probiotic hydrogel can therefore be used as a potential dressing to accelerate wound healing. We expect that this work will provide a new idea for the application of live bacterial therapy in wound healing.

2. Materials and methods

2.1. Materials, bacteria, and cell line

Hyaluronic acid (HA) and dopamine hydrochloride purchased from Aladdin (Aladdin , Shanghai, China) ; LAP purchased from Sigma (Sigma-Aldrich , Shanghai, China); Dulbecco's modified Eagle's medium (DMEM) and Fetal Bovine Serum (FBS) purchased from Gibco (Thermo Fisher Scientific, Shanghai, China), CD206 polyclonal antibody purchased from proteintech (Wuhan, China).

Bacillus velezensis M76T11B (B. velezensis M76T11B) with a high EPS-producing rate was independently screened by our laboratory and conserved in Guangdong Microbial Strain Conservation Centre with the conservation number GDMCC NO: 61384; *Lacticaseibacillus paracasei TYM202 (L. paracasei TYM202)* was independently screened by the laboratory and deposited in Guangdong Microbial Strain Conservation Centre with the conservation number GDMMC NO:62627; *Escherichia coli (E. coli)* and *Staphylococcus aureus (S. aureus)*, conserved in Laboratory 603, School of Light Industry and Food Engineering, Guangxi University.

2.2. Probiotic effects and structural characterization of EPS-M76

2.2.1. Extraction of EPS from B. velezensis M76T11B and evaluation of their proliferative effect

The activated *B. velezensis M76T11B* was inoculated with MRS medium at 5 % inoculum and incubated for 48 h at 37 °C with shaking, then centrifuged at 8000 rpm for 10 min to remove the bacterium, concentrated the supernatant and precipitated the polysaccharide with ethanol. The precipitated polysaccharide was deproteinized with trichloroacetic acid, and the excess trichloroacetic acid was removed by alcohol precipitation and dialysis. Finally, the crude EPS from *B. velezensis M76T11B* (EPS-M76) was obtained by freeze-drying.

Based on previous studies [23], the effect of EPS-M76 on the proliferation of *L. paracasei TYM202* was evaluated in the following 2 media: (i) MRS medium as a normal control (NC); and (ii) EPS medium, MRS medium containing 10 % EPS-M76. All strains were incubated at 37 °C and the growth curve was plotted by measuring the OD_{600} values every 3 h. After 36 h of incubation, the cell viability was confirmed by plate counting on MRS agar, and the content of short-chain fatty acids of supernatant was detected using an HPLC system with an Aminex HPX 87 column (300 mm × 7.8 mm, Bio-Rad Laboratories (Shanghai) Co., Ltd., China) as previously reported [24]. All experiments were performed in triplicate.

2.2.2. Isolation and purification of EPS-M76

EPS-M76 was separated and purified by ion exchange chromatography and gel filtration column chromatography according to Gao et al. [25]. The sample (500 mg) was dissolved in distilled water and then centrifuged. The supernatant was injected into a DEAE-agarose fast flow column (2.6 × 40 cm^2) and eluted with NaCl solution (0–0.6 mol/L, dissolved in 0.02 mol/L Tris-HCl buffer, pH = 7.6) at a flow rate of 1 mL/min. Each tube was collected with 10 mL of eluate. The sugar content of each tube was measured using the phenol-sulphuric acid method. The resulting eluate fractions were concentrated, dialyzed, centrifuged, and loaded onto a Sephacryl S-400 column (1.6 × 100 cm^2, GE Healthcare) and the column was washed with distilled water at a rate of 0.6 mL/min. Each elution peak was collected, concentrated, and lyophilized.

2.2.3. Structural analysis of EPS

The analysis of monosaccharide composition refers to the previous report with some modifications [26]. Briefly, the samples were hydrolyzed with trifluoroacetic acid and later washed five times with methanol. The dried hydrolysate was derivative treated with 1-phenyl-3-methyl-5-pyrazolone and then extracted three times with chloroform. Finally, the aqueous phase was filtered through a 0.22 μm filter and separated on a high-performance liquid chromatograph (Agilent_1260) equipped with an Xbridge C18 column (15 cm × 0.2 mm × 0.25 μm; Waters Co., Milford, MA, USA).

A high-performance liquid chromatography (Agilent_1260) equipped with a RID detector was utilized for molecular weight determination [27]. The TSK-G2500PWXL and TSK-G5000PWXL columns (15 cm × 0.2 mm × 0.25 μm; TOSOH Bioscience, Tokyo, Japan) were used for the separation of polysaccharides. Dextran standards with molecular weights of 1–670 kDa were applied for calibration.

Methylation analysis of polysaccharides according to the methods reported in the literature [28]. In short, 10 mg of polysaccharide and 50 mg of NaOH powder were fully dissolved in 2 ml of anhydrous DMSO, and then methylation was repeated twice with iodomethane. The disappearance of the –OH absorption peak at 3200–3400 cm in the FT-IR spectrum of the polysaccharide indicated that the polysaccharide was completely methylated. The methylated products were hydrolyzed with trifluoroacetic acid, then reduced with NaBH4 and acetylated with acetic anhydride. Finally, the partially methylated alditol acetate (PMAA) was analyzed by GC-MS system using a DB-5MS column (30 m × 0.5 cm × 0.25 μm). The combination of mass spectrometry fragmentation patterns (using the Center for Complex Carbohydrate Research standard database, https://glygen.ccrc.uga.edu/ccrc/specdb/ms/pmaa/pframe.html), monosaccharide composition, and literature data were used to determine the monosaccharide linkage.

The structural information of the polysaccharide was analyzed using NMR spectroscopy. 50 mg of the polysaccharide sample was dissolved in 0.6 mL of deuterium oxide (D2O, 99.9 %). The 1D and 2D NMR spectra were recorded at 25 °C on a Bruker AVANCE III HD500 NMR spectrometer (Bruker Corporation, German).

2.3. Synthesis and determination of mechanical properties of probiotic hydrogels

2.3.1. Modification of polysaccharides

The hyaluronic acid methacrylate was prepared according to previous literature reports [29]. First, 1 g of hyaluronic acid was dissolved in 100 mL of deionized water. Slowly add 4.8 mL of methacrylic anhydride (maintaining the pH of the reaction system at ≈8.0 with NaOH solution) and react with stirring for 24 h. Anhydrous ethanol was then added, centrifuged and the flocculated precipitate was washed 3 times with anhydrous ethanol. The precipitate was dissolved with deionized water, dialyzed (Mw 8000–14000) for 24h, and lyophilized to obtain hyaluronic acid methacrylate (HAMA), which was stored at −20 °C and protected from light.

The dopamine-modified EPS-M76(DAEPS) was synthesized through EDC/NHS coupling chemistry with some modifications [30]. Briefly, 500 mg EPS-M76 was dissolved in 50 mL of phosphate buffer (pH 5.5). 2.5 mmol carbodiimide (EDC) and 2.5 mmol N-Hydroxy succinimide (NHS) were added and stirred for 30 min. Then, 2.5 mmol dopamine hydrochloride was added and stirred under nitrogen protection for 4 h. The solution was dialyzed for 48 h using an 800–14000 Da dialysis bag and lyophilized to obtain the DAEPS.

2.3.2. Preparation of probiotic hydrogels

Firstly, 300 mg of DAEPS was dissolved in 10 mL of PBS solution (pH = 7.2–7.4) containing *L. paracasei TYM202* (10^8 CFU/mL), then 150 mg of HAMA was added to dissolve thoroughly, and finally 25 mg of lithium

phenyl-2,4,6-trimethylbenzoylphosphinate (LAP) was added. The probiotic hydrogel (HAEPS@*L.sei* gel) was obtained by irradiation with 405 nm blue light for 30 s. Probiotic-free HAEPS hydrogel was made in similar steps. HA hydrogel consists of HAMA alone.

2.3.3. Swelling rate

The lyophilized hydrogels were immersed in 0.01 M, pH 7.4 phosphate buffer, and removed at regular intervals at 37 °C. The surface water was removed by filter paper and weighed. The swelling rate of the hydrogel was calculated as follows:

Swelling rate (%) = $(W_b\text{-}W_a)/W_a \times 100$ %

where W_a and W_b are the weights of the hydrogels before and after immersion in PBS respectively. The test was repeated three times for all samples.

2.3.4. Rheology

The energy storage modulus (G′) and loss factor (G″) of hydrogels with a diameter of 40 mm were evaluated with an HR 20 rheometer (TA Instruments - Waters LLC) under the following conditions. (1) Frequency sweep tests of 1–100 rad/s at 37 °C and constant strain (1 %) were carried out. (2) A strain scan test was carried out at 37 °C with a constant frequency of 10 rad/s from 0.1 to 1000 %.

2.4. The microbial activity in the probiotic hydrogel.

2.3.5. Bacterial viability in probiotic hydrogels

The probiotic hydrogel and free probiotics were stored at 4 °C for 0 h, 12 h, and 24 h. Then the live/dead bacteria were stained with SYTO@9 and PI, respectively The number of live/dead bacteria was observed by laser confocal microscope (Olympus FV3000, Japan).

In addition, 1 mL of probiotic-loaded hydrogel (1×10^8 CFU/mL) and an equal number of probiotics were added to 5 mL of MRS and incubated for 24 and 48 h, respectively. The culture medium was collected and the concentrations of organic acids such as lactic acid and acetic acid were determined using an HPLC system equipped with an Aminex HPX 87H column (300 mm × 7.8 mm) [24].

2.3.6. Assessment of bacterial escape ability

The probiotic hydrogel was placed in MRS liquid medium and MRS agar. The culture was incubated at 37 °C. The OD_{600} value of the medium was measured and the escape ability of the bacteria in the hydrogel was observed by taking photographs.

2.4. Biocompatibility and in vitro antibacterial activity of hydrogels

2.4.1. Cytotoxicity assay

The cells were cocultured with hydrogel leachate to evaluate the cytotoxic effect of the prepared hydrogels. L929 cells were inoculated in a 96-well plate (1×10^4 cells/well) for 12h. Then, the original medium was removed and replaced with 100uL of hydrogel leachate. After 24 h of incubation, 10 μL of 5 mg/ml MTT was added and incubated for 4 h. Finally, 200 μL of DMSO was added to each well and the absorbance was measured at 490 nm after shaking for 5 min. The cell survival rate was calculated according to the following formula:

Cell survival rate (%) = $(A_1\text{-}A_0)/A_0 \times 100$ %

where A_0 is the absorbance of the blank wells at 490 nm and A_1 is the absorbance of the experimental wells at 490 nm.

L929 cells cultured with hydrogel extracts were also observed by staining with the Calcein/PI Cell Viability/Cytotoxicity Assay Kit (Beyotime, Shanghai, China).

2.4.2. Hemolysis assay

1 ml of whole mouse blood was added to 1 drop of saturated disodium EDTA solution and centrifuged at 3500 rpm for 5min. The lower erythrocytes were washed 3 times with PBS and then resuspended in 9 mL PBS. 200 μL of hydrogel sample was added to 1 ml of erythrocyte suspension, incubated for 2 h at 37 °C, and 100 μL was taken to measure the OD at 570 nm. PBS and Trition-X100 were used as positive and negative controls.

2.4.3. Scratch wound assays

Migration under different hydrogel leachate treatments was evaluated in confluent cell layers in 12-well plates. The L929 cells were scratched with a 200 μL pipette tip after reaching 80–90 % confluence. After washing with PBS to remove loose cells, 1.5 mL of different serum-free hydrogel leachate was added and incubated at 37 °C. After 0, 12, and 24h, images were obtained and scratch area calculations were performed in four randomly picked fields with Image J software.

2.4.4. Antibacterial activity evaluation

S. aureus and *E. coli* were used to evaluate the antibacterial properties of the hydrogel. Briefly, 0.8 mL of hydrogel was added to the 12-well plate, then 1 mL of bacterial suspension (10^6 GFU/mL) was added to the surface of the hydrogel and the plate was incubated at 37 °C for 12 h. Afterward, the bacteria were suspended by blowing, diluted to the appropriate concentration, and 100ul was applied to the LB plate. The plates were incubated at 37 °C for 18h and then the colonies on the plates were counted. A negative control group without hydrogel was also set up. In addition, the bacterial suspensions were fixed in 2.5 % glutaraldehyde for 3h, then dehydrated in gradient ethanol and observed under the transmission electron microscope (TEM, Hitachi HT7700, Japan) .

2.5. In vivo wound healing on whole-layer skin damage model

All animal experimental protocols were approved by the Institutional Animal Care and Use Committee of Guangxi University, with the animal welfare ethics acceptance number GXU-2022243. Male SD rats (weight 400 ± 20 g) were procured from Si Pei Fu Biotechnology Co., Ltd. (SPF, Beijing, China) and allowed 1 week of acclimatization. Animals were housed in individually ventilated cages under a controlled environment (20–25 °C and relative humidity at 30–70 %). Subsequently, all rats were randomly divided into 4 groups of saline, HA, HAEPS, and HA76 EPS@L.sei according to the different treatments. Each group contained 12 rats. After fasting for 12 h, the rats were intraperitoneally anesthetized. Next, the hair was removed from the back of the rats and a circular defect of 10 mm in diameter was created on the left and right sides of the dorsum. In the HA, HAEPS, and HA76EPS@L.sei groups, the rat wounds were covered with 1 mL of the corresponding hydrogel, which was changed daily, and the saline group was treated with an equal amount of saline. The rats were executed by dislocation after anesthesia 4, 9, and 14 days after surgery, and tissue samples for general analysis were harvested. All tissue sections that were obtained from the rat skin wounds for routine histological examination were stained with H&E Staining. The serum was collected to measure the levels of TNF-α, IL-10, and VEGF-α (ELISA Kit, Nanjing Jiancheng Bioengineering Institute, Jiangsu, China).

2.6. 16S rRNA gene sequencing

16S rRNA gene sequencing was performed based on previous reports [31]. In short, the DNA of collected samples was extracted by the CTAB method. The V3–V4 region of the 16S ribosomal RNA (rRNA) genes were amplified with specific primer 341F (CCTACGGGNGGCWGCAG) and 806R (GACTACHVGGGTATCTAATCC) and barcodes. The Phusion®High-Fidelity PCR Master Mix (New England Biolabs, USA) was used for PCR amplification. PCR products were purified using the DNA Gel Extraction Kit (Qiagen, Germany). Sequencing libraries were constructed with NEBNext® Ultra™ IIDNA Library Prep Kit (New England Biolabs, USA), according to the manufacturer's recommendations. The library was sequenced on an Illumina NovaSeq platform (Illumina, USA) and 250 bp paired-end reads were generated. The obtained data were quality-controlled by FASTP software, and valid tags were obtained by

comparing them with the Silva database. The data is then denoised and filtered to obtain the final amplicon sequence variant. The amplicon Sequence Variables (ASVs) are classified by mapping the Silva database. Finally, ASVs were assigned taxonomy by mapping with the Silva Database.

2.7. Statistical analysis

All experiments were conducted in triplicates independently. Skin microbiome analysis using MicrobiomeAnalyst 2.0, including screening and analysis of differential flora, PCOA analysis, and LDA analysis. The data were expressed as mean ± standard error of the mean (SEM) and were evaluated with the Two-tailed T-test or univariate ANOVA in GraphPad Prism software (version 9.3.1.), visualized by RStudio (version 4.1.1). *$p < 0.05$ and **$p < 0.01$ were considered statistically significant.

3. Results and discussion

3.1. Probiotic effects and structural characterization of EPS-M76

Lactobacilli are probiotics that have many positive effects on human health. Recent research has found that *Lactobacilli* play an important role in wound healing, which is closely related to their strong acid-producing capacity (mainly lactic acid and SCFA) [12,32]. We screened several probiotic strains from fermented foods and found that *L. paracasei TYM202* had the strongest wound healing-promoting effect (Fig. S1). Furthermore, we observed that EPS-M76 promoted the proliferation and metabolism of *L. paracasei TYM202*. Within the EPS group, *L. paracasei TYM202* displayed a heightened growth rate, with a notably higher quantity of viable bacteria observed after 36 h of incubation compared to the control group (Fig. 1, Fig. S2B). In addition, EPS-M76 significantly promoted the production of lactic acid and acetic acid by *L. paracasei TYM202* (Fig. 1 B, Fig. S2A). This indicates that EPS-M76 has excellent prebiotic properties.

Subsequently, a detailed examination of the EPS-M76 structure was conducted to leverage its inherent characteristics more effectively. The crude EPS-M76 were separated based on their charge using a DEAE-Sepharose Fast Flow column. The separation resulted in two fractions: EPS-A and EPS-B (Fig. S2C). These fractions, eluted by DEAE, were further purified on a Sephacryl S-400 column based on molecular weight. The EPS-A exhibited a single elution peak. Although EPS-B presented a double elution peak, we chose its major peak for the next study (Fig. S2 D). The molecular weight distributions confirmed the high purity of these fractions, as depicted in Fig. 1C. The calculated molecular weights for EPS-A and EPS-B were 1.31×10^4 Da and 6.60×10^4 Da, respectively.

The results of monosaccharide composition showed that EPS-A was mainly composed of glucose (83.89 %) and contained a small amount of mannose (8.94 %) and glucuronic acid (7.17 %). EPS-B consisted of mannose (83.85 %), mannuronic acid (11.35 %), and glucose (4.80 %, Fig. 1D–Table S1). This is similar to the results reported by previous publications that the EPS produced by *Bacillus velezensis SN-1* is mainly composed of mannose and glucose [33].

The FT-IR spectra of the two fractions are displayed in Fig. S2E. The absorption band at 3400 cm^{-1} indicated the stretching vibration of –OH

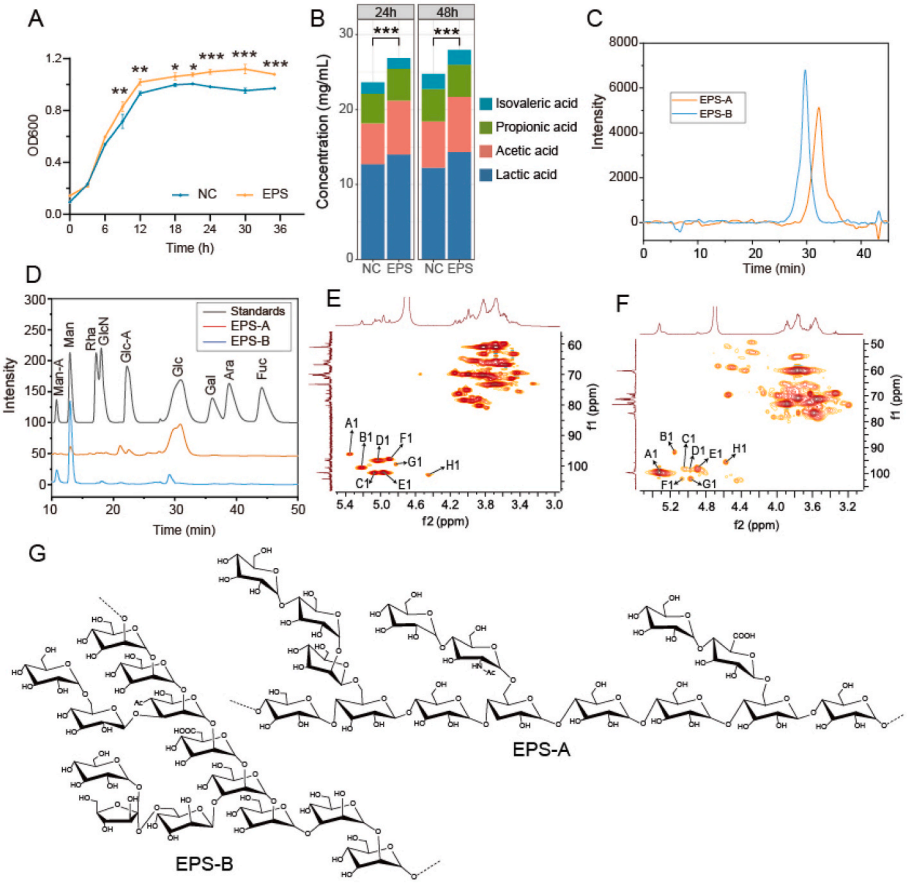

Fig. 1. Probiotic effects and structural characterization of EPS-M76. (A) Growth curve of *L. paracasei TYM202* on different groups. (B) EPS-M76 promotes acid production by *L. paracasei TYM202*. (C) Molecular weight distribution profiles of the three EPS-M76 fragments after purification. (D) Monosaccharide composition of the three EPS-M76 fragments after purification. (E) HSQC spectra of EPS-A. (F) HSQC spectra of EPS-B. (G) Possible repeat units of EPS-A and EPS-B. *p < 0.05, **p < 0.01.

in the constituent sugar residues. The strong band at 2930 cm^{-1} was associated with the stretching vibration of C–H in the sugar ring. The bands at 1400 cm^{-1} and 1650 cm^{-1} indicated the presence of C–H bending vibrations and COO- stretching vibrations [25]. The band at around 1000 cm^{-1} was caused by the vibrations of the C–O. The bands at 930 cm^{-1} and 610 cm^{-1} corresponded to the vibrations of the α-glycosidic and β-glycosidic bonds, respectively [26].

For a deeper understanding of EPS-A and EPS-B structures, methylation analysis was employed to ascertain their glycosidic bond types. As shown in Table S2, EPS-A and EPS-B were composed of six types of glycosidic bond linkages, respectively. EPS-A was mainly composed of (1 → 4) linked glucose (55.67 %), whereas EPS-B was primarily composed of (1 → 2) linked mannose (61.97 %), and both polysaccharides possessed branching structures. The relative content of glycosidic bonds obtained by methylation analysis was consistent with the monosaccharide composition.

Further insights into the structural characteristics of EPS-A and EPS-B were gleaned through NMR spectra (Fig. 1E–F, Figs. S2A–B). The signal at 5.33/99.70 ppm was assigned to H1/C1 of →4)-α-D-Glcp-(1→ [28]. The chemical shifts of H2/C2, and H3/C3 were determined by the crossing signals of COSY and HSQC spectra, registering at 3.56/71.38 ppm, and 3.90/73.20 ppm, respectively. Complemented with the C/H correlation signals from the HMBC spectra, the signals for H4/C4, H5/C5, and H6/C6 were confirmed as 3.58/76.70 ppm, 3.75/71.15 ppm, and 3.77/60.64 ppm, respectively. Signals of the other residues were assigned by the same method. Table S3 summarizes all proton and carbon signals for each sugar residue. The characteristic signals of glyoxylate and acetyl group are not obvious in the ^{13}C spectra, which may be caused by the insufficient scan numbers during the acquisition. However, the cross signals near 175/1.98 ppm in the HMBC spectra, 1.97/24.3 ppm in the HSQC spectra, and the absorption peak at 1650 cm^{-1} in the FT-IR spectra proved the carboxyl and acetyl groups. On the other hand, fructose residues in EPS-B were not detected in the monosaccharide composition analysis as well as methylation analysis, which was caused by the low content of fructose and the easy reduction of fructose to mannose and glucose [34].

Fig. 1G illustrates the possible repeat unit structure of EPS-A and EPS-B, deduced from the results of glycosidic bond analysis and NMR spectroscopy. The EPS-M76 were mainly composed of (1 → 4) linked α-glucose and (1 → 2) linked α-mannose with abundant branched structures. The high abundance of mannose suggests its potential application in assisting microbial to resist external environmental stresses [35]. On the other hand, the branching degree also affects the prebiotic properties of polysaccharides. Generally, polysaccharides with higher branching degrees demonstrate more robust prebiotic effects. EPS-M76 is rich in branches and terminals that are favorable for encapsulating bacteria and being utilized by bacteria. This coincides with that of Wang et al., who reported that rapeseed polysaccharides with higher branching degrees showed better prebiotic activity [36]. Moreover, during the late stages of microbial growth, EPS slows or blocks the entry of stress factors into bacterial cells thus ensuring bacterial viability [37]. These results indicate that EPS-M76 is an excellent candidate for the synthesis of living bacterial hydrogels.

3.2. Characterization of hydrogels

To enhance the gel-forming properties of the polysaccharides, we modified EPS-M76 with dopamine (forming DAEPS) and HA with methacrylic acid (forming HAMA). A new N–H absorption peak near 3080 cm^{-1} for DAEPS and a new C═O absorption peak near 1710 cm^{-1} for HAMA indicate the successful modification of the two polysaccharides (Fig. S3 C, D) [38]. DAEPS and HAMA were utilized to create the initial cross-linking network through hydrogen bonding. Subsequently, under light-induced conditions, a second cross-linking network was established through covalent cross-linking, resulting in the formation of HAMA-enhanced DAEPS multi-crosslinked probiotic hydrogel.

The formation of hydrogels was observed using the test tube inversion method (Fig. 2A), and their FTIR spectroscopy is presented in Fig. 2B. The C═O absorption peak at 1650 cm-1 in the hydrogel was amplified following the addition of DAEPS due to hydrogen bonding formed between DAEPS and HAMA. Interestingly, with the introduction of *L. paracasei TYM202*, the absorption peak at 1550 cm-1 in the hydrogel disappeared, possibly due to interactions such as adsorption, binding, or coagulation of the bacteria with the hydrogel, leading to alterations in the vibrational frequency of COO- in the hydrogel.

Subsequently, we investigated the gelling performance of hydrogels with different concentrations and ratios. HAMA at a concentration of 1.5 % was selected for subsequent study. When increasing the HAMA to DAEPS ratio to 1:2, the hydrogel precursor solution was sufficiently cross-linked and no longer flowed when the tube was tilted, so this ratio was used for subsequent examination (Fig. S4 A). Scanning electron microscopy showed that all hydrogel had a typical cross-linked porous structure with relatively uniform distribution (Fig. 2C). Incorporation of DAEPS decreased the hydrogel pore size, attributed to the formation of hydrogen bonds between DAEPS and HAMA, resulting in a more compact internal structure of the hydrogel. At high magnification, the hydrogel without probiotics exhibited a smooth surface, whereas the probiotics hydrogels displayed a rough surface with uniformly distributed probiotics. The hydrogel did not alter the morphology of the probiotic, *L. paracasei TYM202* maintaining its typical rod-like appearance.

Appropriate viscoelasticity and structural stability of the wound dressing are essential for practical clinical applications [39]. Rheological experiments were conducted to assess hydrogel viscoelasticity (Fig. 2D). The hydrogels were subjected to strain scanning in the range of 0.1–1000 %. In the strain range of 0.1–50 %, both HAEPS and HA EPS@L.sei exhibited reversible elastic deformation, maintaining relatively stable G′ and G″ with G′ consistently higher than G''. As strains higher than 50 %, both hydrogels began to undergo plastic deformation, reaching critical strain points of 193 % and 330 %, respectively. In contrast, HA hydrogels showed strain sensitivity, displaying plastic deformation within the 0.1–3.5 % strain range. These results suggest that the incorporation of DAEPS and probiotics enhanced the hydrogel cross-linking, improving its elastic properties, consistent with the FTIR spectroscopy and scanning electron microscopy results. Li et al. also indicated that the addition of probiotics could enhance the elastic modulus of hydrogels [12]. Frequency scans indicated stable energy storage and loss moduli among the various hydrogels (Fig. 2E). Moreover, all hydrogels exhibited shear-thinning properties, evidenced by decreased viscosity with increasing shear rate (Fig. S4B), a characteristic beneficial for 3D printing inks and injectable hydrogels, ensuring easy extrusion without clogging [40,41].

Hydrogel dressings with superior swelling properties have the potential to accelerate wound healing by absorbing exuded tissue fluid and facilitating tissue consolidation. In this study, we evaluated the swelling properties of hydrogels containing different concentrations of probiotics (0, 10^7, 10^8, and 10^9 CFU/mL) All hydrogels exhibited rapid fluid absorption, with their weight increasing swiftly during the initial phase, reaching a state of swelling equilibrium and maintaining their integrity for up to 200 min (Fig. 2F). Additionally, the probiotic hydrogel exhibited favorable injectability, enabling precise administration using a syringe (Fig. S4C).

In conclusion, these results indicated the favorable mechanical properties and injectability of probiotic hydrogels, positioning them as promising candidates for diverse applications, including wound dressings and tissue engineering.

3.3. The microbial activity in probiotic hydrogel

Excellent microbe-loaded scaffolds should be able to maintain bacterial viability. To assess the activity of *L. paracasei TYM202* encapsulated in probiotic hydrogels, we performed live-dead staining of

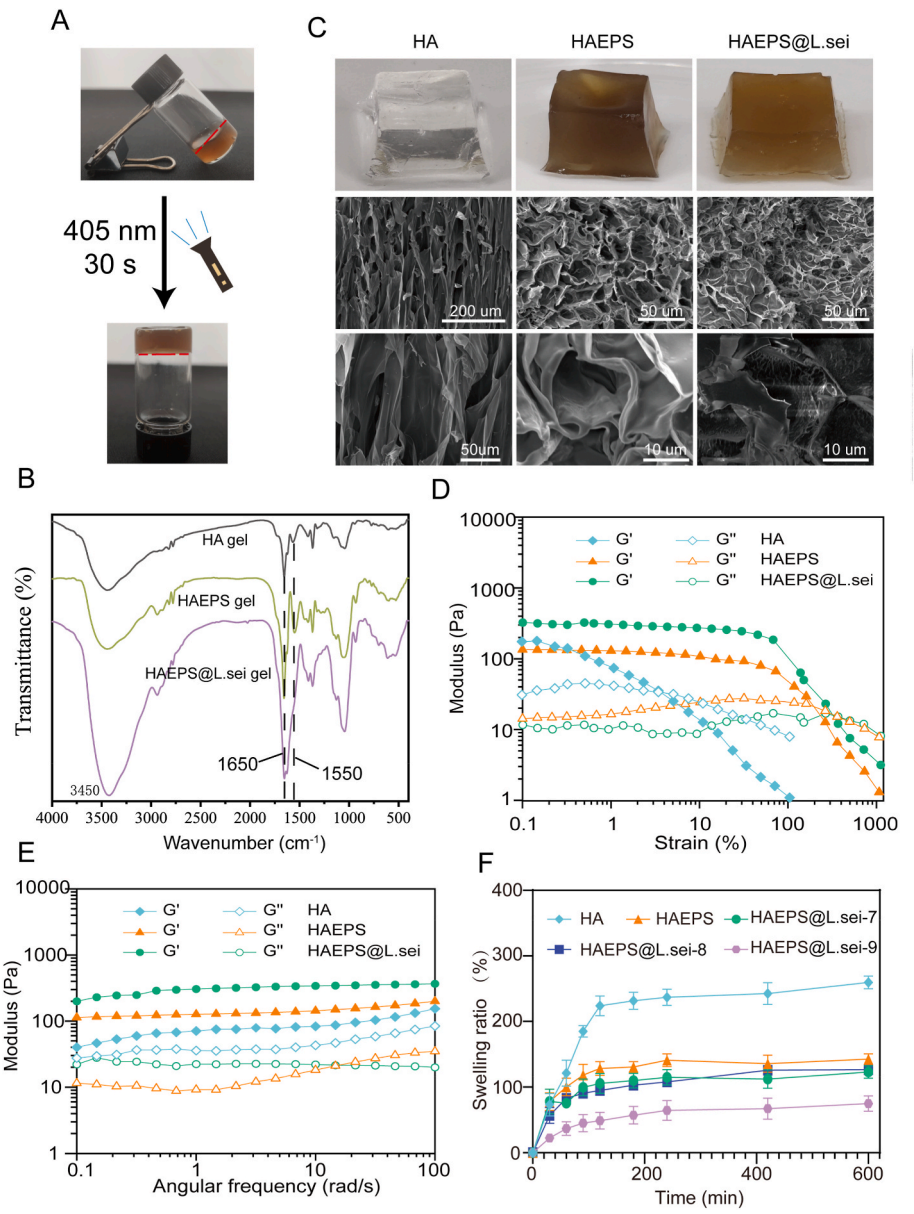

Fig. 2. Characterization of hydrogels. (A) The formation of hydrogels was observed by inversion of the test tube. (B) FT-IR spectra of hydrogels. (C) Pictures of hydrogels and SEM images at different magnifications. (D) Strain-sweep of hydrogel. (E) Frequency-sweep of hydrogels. (F) Swelling rates of different hydrogels.

probiotics after storing the probiotic hydrogels and equal numbers of free *L. paracasei TYM202* at 4 °C for different times. The results demonstrated the superior efficacy of the hydrogel in maintaining probiotic activity. The bacterial death ratio of probiotics loaded in hydrogels stabilized at approximately 20 % within 24 h, significantly lower than that of free probiotics (Fig. 3A and B). Z-axis scanning of the probiotic hydrogels showed that the probiotics were uniformly distributed in the hydrogels (Fig. S5A).

The protective effect of hydrogel on probiotics can be attributed to several factors. Firstly, HA constitutes the primary component of the extracellular matrix, while EPS-M76 exhibits confirmed probiotic activity, thus the scaffolds of hydrogel we developed can provide a conducive environment and nutrients for bacterial cells. The three-dimensional network structure of hydrogel provides a large amount of growth space for bacteria, and the bacteria encapsulated in the hydrogel matrix are less affected by the stress factors and conditions in the surrounding environment [42]. Moreover, this three-dimensional growth condition also facilitates the exchange of substances between bacteria and the environment. Thirdly, it has been reported that the EPS wrapped around the bacteria can slow down or prevent the entry of stress factors into the bacterial cells, which is therefore more favorable for the survival of the bacteria [37].

Next, we further verified the bacterial activity by testing the acid-producing ability of the probiotics. The lactic and acetic acid production capacity of probiotics loaded in the hydrogel was significantly enhanced compared to free probiotics (Fig. 3C, Fig. S5B). This further demonstrates that our protocol ensures bacterial viability and is a viable alternative to existing live bacterial treatment protocols.

It is worth noting that the probiotics encapsulated in the hydrogel only grew within the interior and surface of the hydrogel. After 12 h of incubation, the OD600 of the medium remained at the same level as the blank MRS medium (Fig. 3D, Fig. S5C). Incubating the probiotic hydrogel on MRS plates for 12 h did not reveal any *L. paracasei TYM202* presence surrounding the hydrogel demonstrating the superb encapsulation ability of the hydrogel. This can be attributed to the strong adhesion of dopamine in DAEPS to probiotics, preventing probiotics from escaping and avoiding potential microbial threats [43].

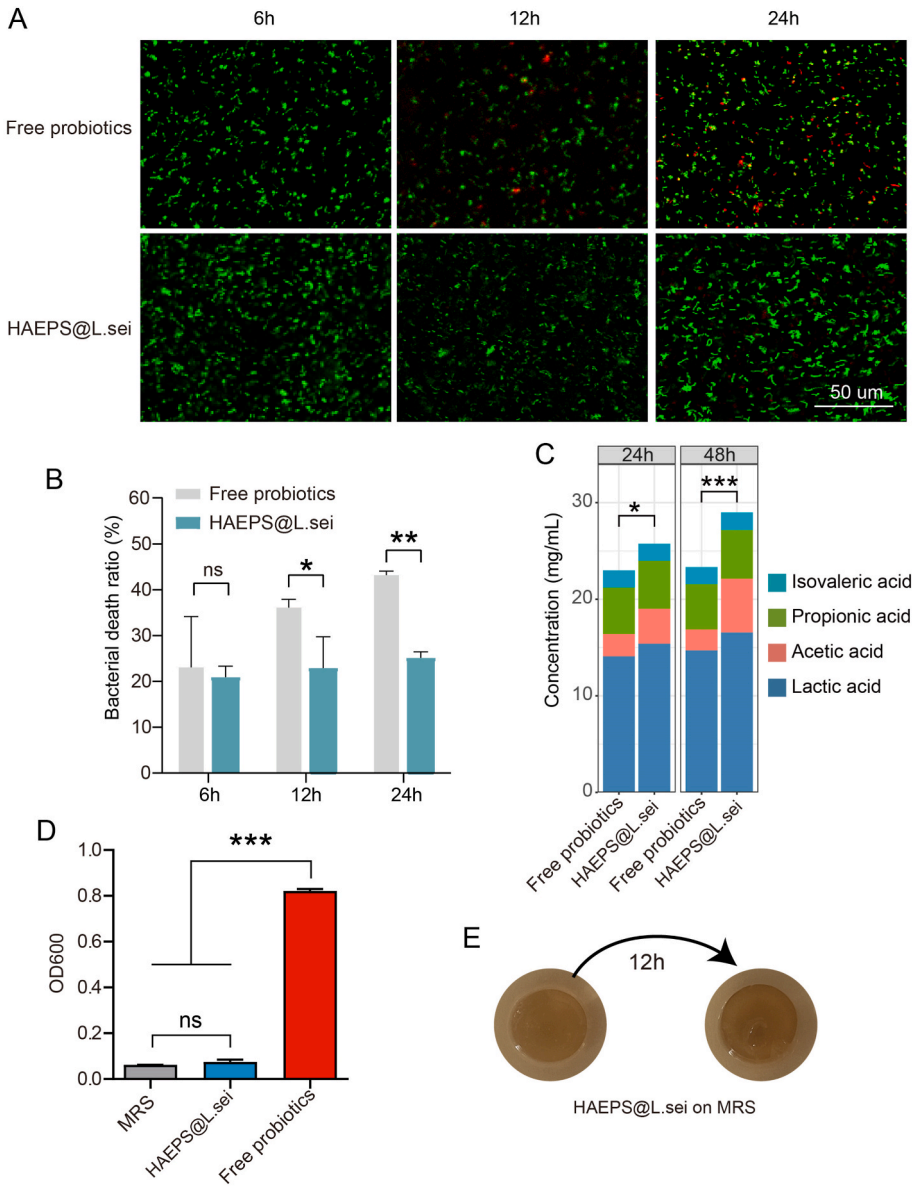

Fig. 3. The microbial activity in the probiotic hydrogel. (A) Live/dead bacterial staining images of probiotic hydrogels and free bacteria after different times of storage at 4 °C (scale bar, 50 μm). (B) The percentage of dead bacteria calculated based on fluorescence intensity. (C) Measurement of acid-producing ability of probiotic hydrogel. (D) OD600 of the culture medium of probiotic hydrogel after 12h incubation in MRS. (E) Probiotic hydrogels incubated on MRS plates for 12h. Bar graphs represent as mean ± SEM. *p < 0.05, **p < 0.01.

3.4. Biocompatibility and in vitro antibacterial activity of hydrogels

The biocompatibility of hydrogels is a critical consideration for their clinical application in wound dressings. To evaluate the biocompatibility, L929 cells were incubated with different hydrogel leachate. Live-dead staining results indicated no significant differences in cell density, spreading area, or the number of live-dead cells between the HAEPS and HAEPS@L.sei groups and the control group (Fig. 4A). Cytotoxicity assessments via the MTT assay indicated mild cytotoxicity in HA hydrogel leachates at higher concentrations (100, 50 mg/mL), resulting in a cell survival rate of about 70 %. However, probiotic hydrogels exhibited remarkable cytocompatibility, with cell survival rates approaching 100 % at leachate concentrations below 100 mg/mL, regardless of increased probiotic content. At a concentration of 10 mg/mL, the hydrogel leachate showed enhanced cell viability, indicating its potential to promote cell proliferation.

Next, hemolysis assays were performed to further evaluate hydrogel hemocompatibility, as the wound dressing inevitably contact with blood. The co-incubation of the hydrogel with erythrocyte suspension did not result in any significant hemolysis, with absorbance at 570 nm being consistently below 0.2, comparable to the negative control of PBS (Fig. 4C). Considering both biocompatibility and mechanical properties across various concentrations of probiotic hydrogels, a final probiotic concentration of 10^8 CFU/mL was selected for subsequent studies.

The in vitro wound closure effect of the probiotic hydrogel was verified through a scratch assay using L929 cells. At 12 h, wound healing was observed in the HAEPS and HAEPS@L.sei groups (Fig. 4D). By 24h, the mean wound closure rate in the HAEPS2 group was notably higher than the control group (Fig. 4E). Furthermore, the in vitro antibacterial activity of the hydrogel was then evaluated with *S.s aureus* and *E. coli*. As shown in Fig. 4F, the HAEPS@L.sei exhibits a stronger effect than HAEPS without probiotic bacteria. The two pathogenic bacteria treated with the hydrogel were observed under transmission electron microscopy after fixation and ethanol dehydration. The cell membranes of the

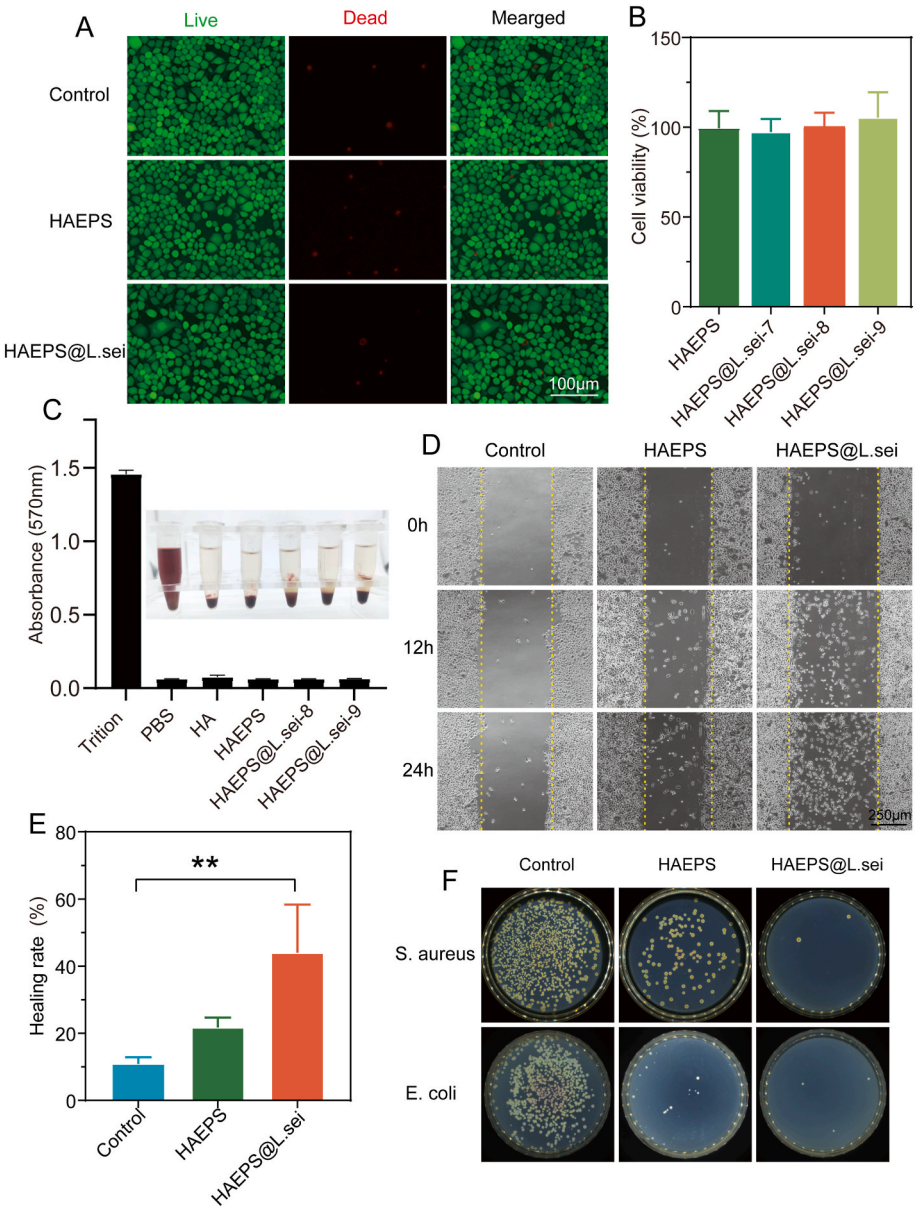

Fig. 4. Biocompatibility and in vitro antibacterial activity of hydrogels. (A) Confocal microscopy images of a live/dead assay of L929 cells cultured for 24 h with 20 mg/ml of hydrogel leachate (Scale bar, 100 μm). (B) The viability of L929 cells measured by MTT after 24h incubation with 20 mg/ml of hydrogel leachate. (C) Blood compatibility of the hydrogel. (D) Photographs of in vitro cell scratching assay, the yellow dotted indicates the starting scratch area (Scale bar, 250 μm). (E) The healing rate of each group of scratches at 24h after scratching. (F) The number of pathogenic bacteria in different hydrogel treatment groups after 12 h of co-culture with hydrogel. Bar graphs represent as mean ± SEM. *$p < 0.05$, **$p < 0.01$.

control group were intact and smooth, while those of the HAEPS-treated bacteria were crumpled, and those of the HAEPS@L.sei-treated bacteria were deformed or even ruptured (Fig. S6B). The excellent antibacterial properties of the probiotic hydrogel are due to the lactic acid and antibacterial agents secreted by *L. paracasei TYM202*, which inhibit the growth of pathogenic bacteria [44]. Taken together, these results suggest that probiotic hydrogels are biocompatible, non-hemolytic, promote cell proliferation and migration, and possess antibacterial activity.

3.5. *Effects of the probiotic hydrogel on rat full-thickness skin injury model in vivo*

To evaluate the efficacy of probiotic hydrogels on wound healing, we applied HA, HAEPS, and HAEPS@L.sei hydrogels to full-thickness skin wounds in SD rats, with saline-treated wounds serving as controls. Wound tissue was collected and photographed on days 0, 4, 9, and 14. Gross observations of rat wounds showed a significant reduction in the size of the probiotic hydrogel-treated wounds, particularly on days 9 and 14(Fig. 5A). We further quantified the wound closure healing rate in all groups (Fig. 5B). By day 9, wounds treated with HAEPS@L.sei showed significantly higher closure rates compared to the other three groups ($p < 0.05$). By day 14, the mean wound healing rates were 84.5 % (Control), 88.1 % (HA), 90.6 % (HAEPS), and 96.47 % (HAEPS@L.sei) respectively, indicating that the probiotic hydrogel (HAEPS@L.sei) demonstrating markedly faster wound healing compared to other treatments ($p < 0.05$).

Histomorphometric evaluation of the wound healing efficacy of the hydrogels was conducted via H&E staining (Fig. 5C). On days 9 and 14, all hydrogel-treated groups exhibited dense granulation tissue, along with the formation of new epidermis and dermis (indicated by green arrows). Notably, wounds treated with HAEPS@L.sei almost completely healed after 14 days, displaying typical histological structures similar to

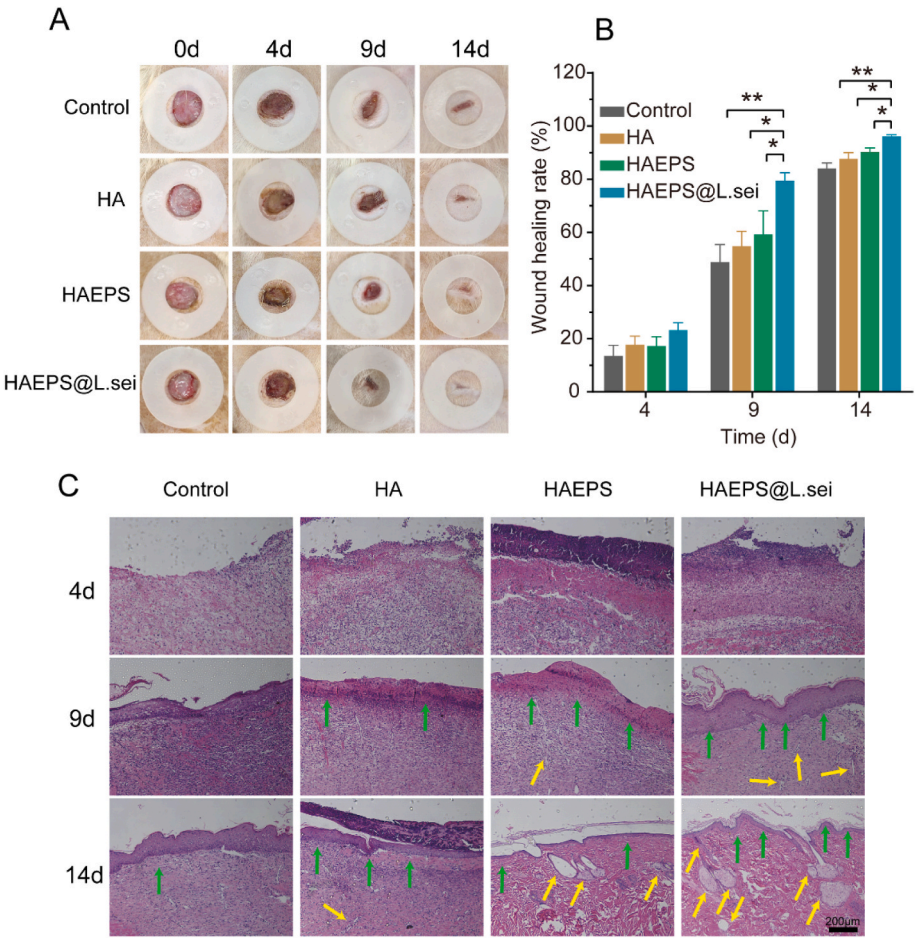

Fig. 5. Effects of the probiotic hydrogel on rat full-thickness skin injury model in vivo. (A) Representative photographs of the wound healing process in different treatment groups. (B) The wound healing rate of each treatment group at different times. (C) H&E staining of wound tissues at various time points. Green arrows indicate the newly formed epidermis and dermis, yellow arrows indicate newly formed skin appendages (scale bar, 200 μm). Bar graphs represent as mean ± SEM.*$p < 0.05$, **$p < 0.01$.

intact skin, notably with a higher number of well-developed skin appendages including hair follicles and blood vessels (highlighted by yellow arrows). Furthermore, the HAEPS@L.sei group exhibited a notable decrease in the number of inflammatory cells during the healing process compared to the other treatment groups. Taken together, the results demonstrate that the HAEPS@L.sei hydrogel has superior wound healing ability.

3.6. Collagen deposition and the expression of inflammatory factors during the healing process.

Wound healing is one of the most complex processes in the body and consists of three overlapping but distinct phases: inflammatory, proliferative, and remodeling [45]. The inflammatory phase is accompanied by the infiltration of large numbers of inflammatory cells and the secretion of high levels of inflammatory factors. To investigate the mechanism underlying probiotic hydrogels-mediated wound healing, we measured the distribution of anti-inflammatory macrophages (M2, CD206-labelled, red) and pro-inflammatory macrophages (M1, CD80-labelled, green) in the wound tissue during the inflammatory phase (day 4) using immunofluorescence. Results showed significantly higher levels of M2 macrophages in the HAEPS@L.sei group compared to other groups, while M1 macrophages were significantly lower than in the control group ($p < 0.01$) (Fig. 6A–C). We also measured the serum levels of inflammatory factors IL-10 and TNF-α in rats at day 4 by enzyme-linked immunoassay. The results showed that the levels of the anti-inflammatory factor IL-10 were significantly higher in the HA EPS@L.sei group ($p < 0.01$) than the other group, and the levels of the pro-inflammatory factor TNF-α were significantly lower in the HA EPS@L.sei group than the control group, consistent with the immunofluorescence results (Fig. 6 E, F). This effect was attributed to lactic acid released by *L. paracasei TYM202* encapsulated in the hydrogel, which was reported as a metabolite signaling molecule that induces a shift from M1 to M2 phenotype in macrophages [46]. It has been reported that high concentrations of lactic acid inhibit glycolysis in immune cells, decreasing the rate of extracellular acidification and increasing the rate of oxygen consumption, which responds to the metabolic state with an anti-inflammatory response to inhibit inflammation [47].

Lactate-induced M2 macrophages also promote angiogenesis by secreting anti-inflammatory mediators and releasing angiogenic factors, which are essential in the proliferative phase for maintaining fibroblast proliferation, collagen synthesis, and epithelial regeneration [48,49]. Therefore, we next evaluated the expression of the vascular endothelial growth factor α(VEGF-α) at the proliferative phase (day 9). Serum VEGF-α levels were significantly higher ($P < 0.05$) in the HAEPS@L.sei group, indicating the probiotic hydrogel promoted vascular regeneration of the wound (Fig. 6G).

During the remodeling phase, collagen deposition plays a pivotal role in facilitating healing [50]. Masson staining analysis indicated a notable increase in collagen deposition within the hydrogel-treated group, particularly evident in the HAEPS@L.sei-treated group where the collagen volume fraction surpassed significantly that of the control and HA groups (Fig. 6A–G). In addition, the probiotic hydrogel effectively regenerates skin appendages while promoting wound healing, resulting

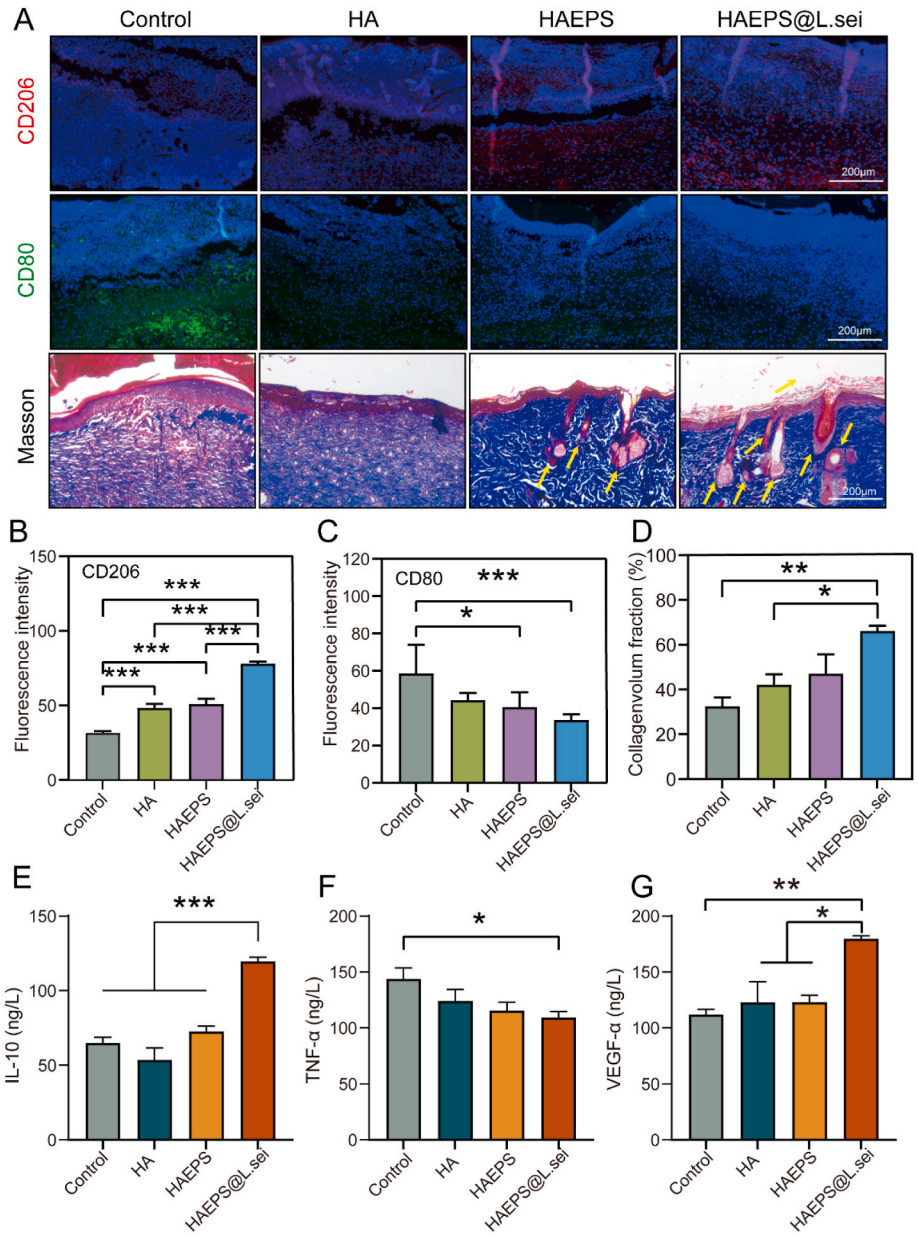

Fig. 6. Collagen deposition and the expression of inflammatory factors during the healing process. (A) Immunofluorescence staining for CD206, and CD80 at day 4, and Masson trichrome staining at day 14 (scale bar, 200 μm). Fluorescence intensity of CD206 (B) and CD80 (C) in the inflammatory phase of day 4. (D) Collagen area fraction in the remodeling phase of day 14. Serum IL-10 levels (E) and TNF-α levels (F) in the inflammatory phase of day 4. (G) Serum VEGF-α levels during the proliferative phase of day 9. Bar graphs represent as mean ± SEM. *$p < 0.05$, **$p < 0.01$.

in healed tissue that is consistent with healthy skin. In summary, the above results suggest that probiotic hydrogels facilitate a shift of macrophages from the M1 phenotype to the M2 phenotype, thereby reducing inflammation occurrence during wound healing, and concurrently promoting angiogenesis and collagen deposition, ultimately expediting the wound healing process.

3.6. Skin microbiota analysis during wound healing

Similar to gut microbiota, skin microbiota play an important role in protecting the host from pathogens and in regulating the immune system [51]. Skin is exposed to a complex external environment daily, but the composition of the microbial community remains in a strikingly similar state. However, disturbances in the equilibrium between skin microbiota and the host can adversely impact the host, leading to various diseases [2,52]. To investigate the effect of probiotic hydrogels on wound skin microbiota, we performed 16S rRNA sequencing of the skin microbiota in both the control and probiotic hydrogel groups, comparing them with the original skin microbiota of rats. Principal coordinate analysis (PCoA) at the genus level revealed differences in skin microbiota composition between the saline-treated C-4d group and the original rat skin microbiota (Original group) on the early post-skin injury period (postoperative day 4), with the former displaying lower *Firmicutes* and higher *Proteobacteria* at the phylum level (Fig. 7A–B). Conversely, the probiotic hydrogel-treated group maintained a high similarity to the skin microbiota of the Original group. This aligns with findings by Assarsson et al., indicating a significant reduction in the abundance of phylum *Firmicutes* in skin with psoriasis compared to normal skin [53]. For the detailed difference in skin microbiota between the Original and C-4d groups, a total of 17 genus-level differential bacteria were identified by linear discriminant analysis (LDA, $|LDA| > 2$, $p < 0.05$, Fig. 7C). In the C-4d group, notably increased *Enterobacter* and

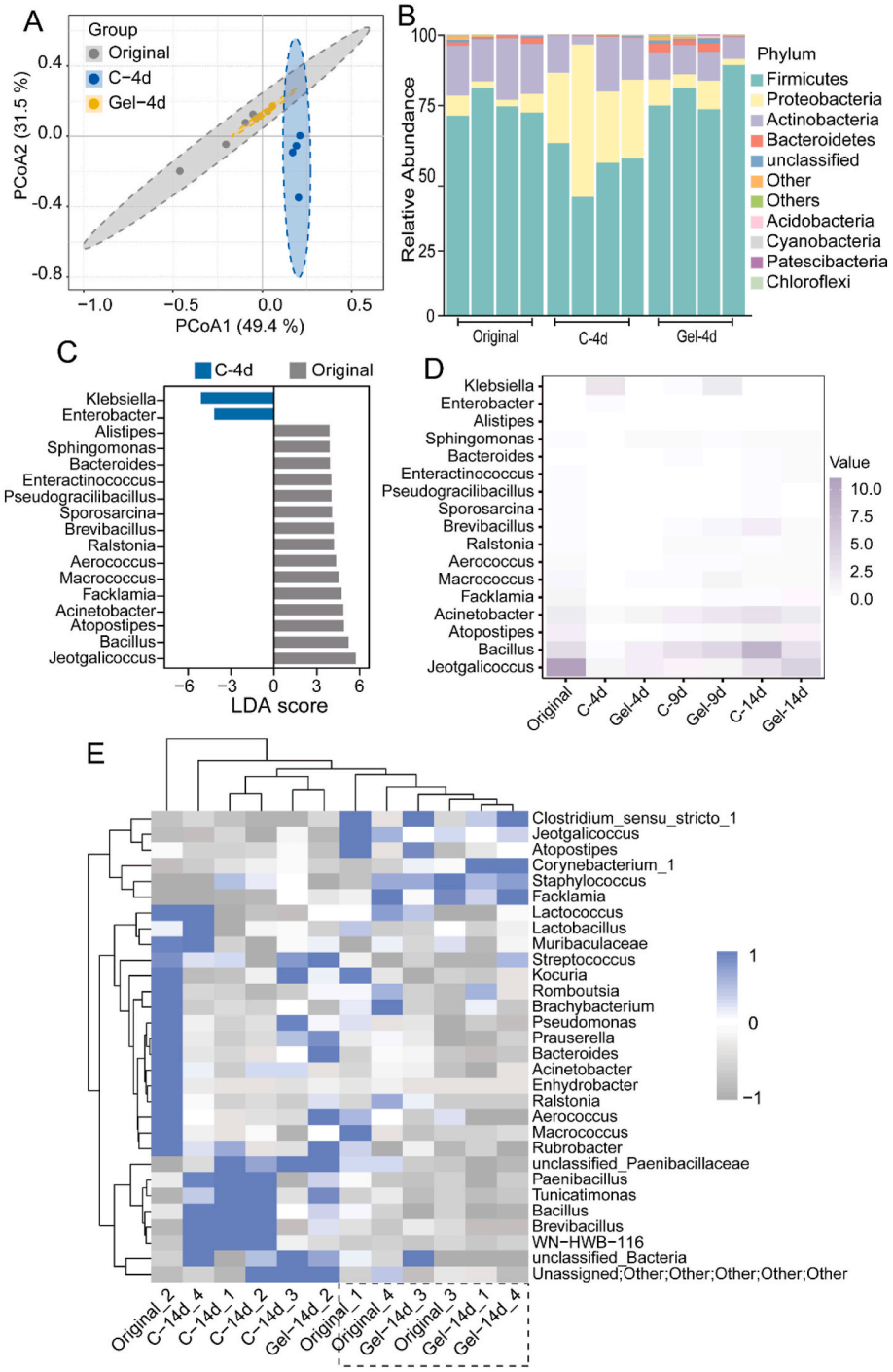

Fig. 7. Skin microbiota analysis during wound healing. (A) Principal coordinate analysis (PCoA) plots of skin microbiota composition in the Original, Control, and Probiotic hydrogel groups at day 4. (B) Skin microbiota composition at the phylum level for the Original, Control, and Probiotic hydrogel groups at day 4. (C) Linear discriminant analysis (LDA) effect size method was performed to compare enriched taxa (levels of genus) between the two groups. The bar plot listed the significantly differential taxa ($p < 0.05$) in the Original and C-4d groups. (D) Relative abundance of differential genera in the Original and C-4d groups during healing in each group. (E) Heat map of clustering of the top 30 genera in abundance for each group during healing.

Klebsiella, along with decreased *Jeotgalicoccus*, were observed compared to the Original group. Subsequent analysis of the mean abundance of these differential bacteria showed that the probiotic hydrogel-treated group exhibited similar bacteria abundance to the Original group during wound healing process, while the saline-treated control group showed a slower recovery as the wound healed (Fig. 7D). Additionally, POCA analysis demonstrated that the saline-treated control group only clustered with the original skin microbiota by day nine, whereas the probiotic hydrogel-treated group maintained a highly similar skin microbiota structure to that of the original skin throughout the wound healing process (Figs. S7A–B). This suggests that HAEPS@L.sei hydrogels can maintain a stable skin microbiota structure. Clustering analysis of the top 30 bacteria in abundance at the genus level on postoperative day 14 showed that the Gel-14d group closely clustered with the Original group (Fig. 7E), further confirming that the probiotic hydrogel maintained the structure of the wound microbiota. Notably, the

abundance of *Lactobacilli* in the wound in the probiotic hydrogel-treated group remained at the same level as the original and blank groups during wound healing, indicating that the probiotic bacteria loading in the hydrogel were not released, which is the same as the previous results (Fig. S7C).

L. paracasei TYM202 encapsulated in hydrogels are a rich source of short-chain fatty acids (SCFA). SCFA can modulate the production of cellular immune factors (TNF-α, IL-6, IL-10), activate resident skin regulatory T cells, and attenuate inflammatory responses, which helps maintain skin homeostasis [54]. On the other hand, the probiotic hydrogel exhibited significant effectiveness against *E. coli* and *S. aureus*, indicating its ability to prevent exogenous pathogenic bacteria and reduce the production of their toxic metabolites. In addition, the skin microbiota is influenced by environmental factors such as pH, humidity, and light. pH is critical for skin permeability barrier homeostasis, keratinocyte desquamation, and other functions. The pH of normal skin is slightly acidic, ranging from 4 to 6, while infected wounds have an alkaline pH [55]. Macrophage responses, fibroblast proliferation, angiogenesis, collagen synthesis, and DNA formation require the acidic conditions of the wound to facilitate wound closure [56]. *L. paracasei TYM202* produced short-chain fatty acids, lactic acid, and other organic acids that maintain the slightly acidic environment of the skin. Additionally, HAEPS@L.sei hydrogels provide constant humidity, which helps the skin to maintain water balance. And EPS-M76, which acts as a prebiotic, protects probiotics and promotes their growth. In conclusion, the probiotic hydrogel provides a favorable environment for the skin microbiota to survive and thus maintains the stability of the skin microbiota. This facilitates the normal performance of various cellular functions and thus promotes wound healing.

4. Conclusion

In summary, we successfully prepared a probiotic hydrogel by dopamine modification of probiotic-preferred EPS-M76, followed by the introduction of hyaluronic acid methacrylate into the EPS matrix and encapsulating *L. paracasei TYM202*. The M76-EPS in the probiotic hydrogel exhibited prebiotic properties, effectively maintaining the activity of the probiotic bacteria and promoting the growth and metabolism of *L. paracasei TYM202*. The probiotic hydrogel exhibits favorable mechanical properties and biocompatibility, making it a promising candidate for clinical wound dressing applications. Our results demonstrated that the probiotic hydrogel could stimulate macrophage polarization towards the M2 phenotype and accelerate the three phases of wound repair (inflammation, proliferation, and remodeling phases). In addition to its immunomodulatory function, probiotic hydrogel protects the wound from pathogenic bacterial infections while providing favorable conditions for the skin microbiota to survive and thus maintain the homeostasis of the wound microbiota. We expect that this work will provide a new idea for the application of live bacterial therapy in wound healing.

Data availability

The data that support the findings of this study are available from the corresponding author upon reasonable request.

Ethics approval and consent to participate

All animal experimental protocols were approved by the Institutional Animal Care and Use Committee of Guangxi University, with the animal welfare ethics acceptance number GXU-2022243. All participants consented to publish the paper.

CRediT authorship contribution statement

Hongtao Xu: Data curation, Investigation, Methodology, Writing – original draft. **Yaqian Li:** Data curation, Methodology, Software. **Jiangping Song:** Data curation, Methodology, Software. **Liuyang Zhou:** Data curation, Methodology, Software. **Kaizhang Wu:** Data curation, Methodology, Software. **Xingyu Lu:** Data curation, Methodology, Software. **XiaoNing Zhai:** Software, Visualization. **Zhili Wan:** Funding acquisition, Writing – review & editing. **Jie Gao:** Funding acquisition, Supervision, Validation, Writing – review & editing.

Declaration of competing interest

The authors declare that they have no known competing financial interests or personal relationships that could have appeared to influence the work reported in this paper.

Acknowledgments

This study was supported by the National Natural Science Foundation of China (grant number: 32001696), Guangxi Science and Technology Base and Talent Special Project (grant number: 2021AC19445), National Natural Science Foundation of China (grant number: 32172347), and the Natural Science Foundation of Guangdong Province (grant number: 2021A1515011000).

Appendix A. Supplementary data

Supplementary data to this article can be found online at https://doi.org/10.1016/j.bioactmat.2024.01.011.

References

[1] M. Habeebuddin, R.K. Karnati, P.N. Shiroorkar, S. Nagaraja, S.M.B. Asdaq, M. K. Anwer, S. Fattepur, Topical probiotics: more than a skin deep, Pharmaceutics 14 (3) (2022) 557, https://doi.org/10.3390/pharmaceutics14030557.
[2] T.A. Harris-Tryon, E.A. Grice, Microbiota and maintenance of skin barrier function, Science 376 (6596) (2022) 9940–9945, https://doi.org/10.1126/science.abo0693.
[3] A.L. Byrd, Y. Belkaid, J.A. Segre, The human skin microbiome, Nat. Rev. Microbiol. 16 (3) (2018) 143–155, https://doi.org/10.1038/nrmicro.2017.157.
[4] Y.E. Chen, M.A. Fischbach, Y. Belkaid, Skin microbiota-host interactions (vol 553, pg 427, Nature 555 (7697) (2018) 427–436, https://doi.org/10.1038/nature25994, 2018.
[5] A. Farazin, Z. Torkpour, S. Dehghani, R. Mohammadi, M.D. Fahmy, S. Saber-Samandari, K. Adel Labib, A. Khandan, A review on polymeric wound dress for the treatment of burns and diabetic wounds, Int. J. Biodivers. Sci. Manag. 6 (2) (2021) 44–50, https://doi.org/10.34172/ijbsm.2021.08.
[6] S.Q. Li, S.J. Dong, W.G. Xu, S.C. Tu, L.S. Yan, C.W. Zhao, J.X. Ding, X.S. Chen, Antibacterial hydrogels, Adv. Sci. 5 (5) (2018) 1700527, https://doi.org/10.1002/advs.201700527.
[7] Z.Z. Ming, L. Han, M.Y. Bao, H.H. Zhu, S.J. Qiang, S.B. Xue, W.W. Liu, Living bacterial hydrogels for accelerated infected wound healing, Adv. Sci. 8 (24) (2021), https://doi.org/10.1002/advs.202102545.
[8] L. Yang, Z. Han, C.H. Chen, Z.Y. Li, S.P. Yu, Y. Qu, R. Zeng, Novel probiotic-bound oxidized *Bletilla striata* polysaccharide-chitosan composite hydrogel, Mater. Sci. Eng., C 117 (2020), https://doi.org/10.1016/j.msec.2020.111265.
[9] Y. Ito, M. Amagai, Controlling skin microbiome as a new bacteriotherapy for inflammatory skin diseases, Inflamm. Regen. 42 (1) (2022) 26, https://doi.org/10.1186/s41232-022-00212-y.
[10] H.M. Ju, H. Chen, A.N. Xiang, Y.W. Wang, T.L. Yue, Y.H. Yuan, Identification and characterization of Lactobacillus paracasei strain MRS-4 antibacterial activity against Alicyclobacillus acidoterrestris, LWT–Food Sci. Technol. 150 (2021) 111991, https://doi.org/10.1016/j.lwt.2021.111991.
[11] K. Bendjeddou, M. Fons, P. Strocker, D. Sadoun, Characterization and purification of a bacteriocin from Lactobacillus paracasei subsp paracasei BMK2005, an intestinal isolate active against multidrug-resistant pathogens, World J. Microbiol. Biotechnol. 28 (4) (2012) 1543–1552, https://doi.org/10.1007/s11274-011-0958-1.
[12] L. Mei, D.J. Zhang, H.R. Shao, Y.P. Hao, T. Zhang, W.P. Zheng, Y.J. Ji, P.X. Ling, Y. Lu, Q.H. Zhou, Injectable and self-healing probiotics-loaded hydrogel for promoting superbacteria-infected wound healing, ACS Appl. Mater. Interfaces 14 (18) (2022) 20538–20550, https://doi.org/10.1021/acsami.1c23713.
[13] S.J. Yu, H.C. Sun, Y.G. Li, S. Wei, J.Y. Xu, J.Q. Liu, Hydrogels as promising platforms for engineered living bacteria-mediated therapeutic systems, Mater, Today Bio 16 (2022) 11, https://doi.org/10.1016/j.mtbio.2022.100435.
[14] O.A. Praepanitchai, A. Noomhorm, K. A, Anal, survival and behavior of encapsulated probiotics (Lactobacillus plantarum) in calcium-alginate-soy protein isolate-based hydrogel beads in different processing conditions (pH and temperature) and in pasteurized mango juice, BioMed Res. Int. 2019 (2019), https://doi.org/10.1155/2019/9768152.

[15] E. Ahmadian, A. Eftekhari, D. Janas, P. Vahedi, Nanofiber scaffolds based on extracellular matrix for articular cartilage engineering: a perspective, Nanotheranostics 7 (1) (2023) 61–69, https://doi.org/10.7150/ntno.78611.
[16] J.L. Patarroyo, J.S. Florez-Rojas, D. Pradilla, J.D. Valderrama-Rincón, J.C. Cruz, L. H. Reyes, Formulation and characterization of gelatin-based hydrogels for the encapsulation of Kluyveromyces lactis-applications in packed-bed reactors and probiotics delivery in humans, Polymers 12 (6) (2020), https://doi.org/10.3390/polym12061287.
[17] X. Alvarez, A. Alves, M.P. Ribeiro, M. Lazzari, P. Coutinho, A. Otero, Biochemical characterization of Nostoc sp. exopolysaccharides and evaluation of potential use in wound healing, Carbohydr. Polym. 254 (2021) 117303, https://doi.org/10.1016/j.carbpol.2020.117303.
[18] X.M. Wang, M.J. Xu, D.L. Xu, K. Ma, C.L. Zhang, G.X. Wang, M.S. Dong, W. Li, Structural and prebiotic activity analysis of the polysaccharide produced by Lactobacillus helveticus SNA12, Carbohydr. Polym. 296 (2022) 119971, https://doi.org/10.1016/j.carbpol.2022.119971.
[19] M.Z. Wang, W.Y. Zhou, Y. Yang, J.R. Xing, X.D. Xu, Y.Q. Lin, Potential prebiotic properties of exopolysaccharides produced by a novel *Lactobacillus* strain, *Lactobacillus pentosus* YY-112, Food Funct. 12 (19) (2021) 9456–9465, https://doi.org/10.1039/d1fo01261d.
[20] H. Pourjafar, F. Ansari, A. Sadeghi, S.A. Samakkhah, S.M. Jafari, Functional and health-promoting properties of probiotics' exopolysaccharides; isolation, characterization, and applications in the food industry, Crit. Rev. Food Sci. Nutr. 63 (26) (2023) 8194–8225, https://doi.org/10.1080/10408398.2022.2047883.
[21] A. Bibi, Y.A. Xiong, M.S.R. Rajoka, H.M. Mehwish, E. Radicetti, M. Umair, M. Shoukat, M.K.I. Khan, R.M. Aadil, Recent advances in the production of exopolysaccharide (EPS) from *Lactobacillus* spp. and its application in the food industry: a review, Sustainability 13 (22) (2021), https://doi.org/10.3390/su132212429.
[22] W. Kansandee, D. Moonmangmee, S. Moonmangmee, P. Itsaranuwat, Characterization and Bifidobacterium sp. growth stimulation of exopolysaccharide produced by *Enterococcus faecalis* EJRM152 isolated from human breast milk, Carbohydr. Polym. 206 (2019) 102–109, https://doi.org/10.1016/j.carbpol.2018.10.117.
[23] F. Zhou, X.Y. Jiang, T. Wang, B.L. Zhang, H.F. Zhao, Lycium barbarum polysaccharide (LBP): a novel prebiotics candidate for bifidobacterium and Lactobacillus, Front. Microbiol. 9 (2018) 11, https://doi.org/10.3389/fmicb.2018.01034.
[24] O. Hernandez-Hernandez, G.L. Côté, S. Kolida, R.A. Rastall, M.L. Sanz, In vitro fermentation of alternansucrase raffinose-derived oligosaccharides by human gut bacteria, J. Agric. Food Chem. 59 (20) (2011) 10901–10906, https://doi.org/10.1021/jf202466s.
[25] J. Gao, L.Z. Lin, B.G. Sun, M.M. Zhao, Comparison study on polysaccharide fractions from laminaria japonica: structural characterization and bile acid binding capacity, J. Agric. Food Chem. 65 (44) (2017) 9790–9798, https://doi.org/10.1021/acs.jafc.7b04033.
[26] J. Gao, L.Z. Lin, B.G. Sun, M.M. Zhao, A comparison study on polysaccharides extracted from Laminaria japonica using different methods: structural characterization and bile acid-binding capacity, Food Funct. 8 (9) (2017) 3043–3052, https://doi.org/10.1039/c7fo00218a.
[27] L. Tian, H. Gruppen, H.A. Schols, Characterization of (Glucurono)arabinoxylans from oats using enzymatic fingerprinting, J. Agric. Food Chem. 63 (50) (2015) 10822–10830, https://doi.org/10.1021/acs.jafc.5b04419.
[28] Y. Zhang, X.L. Pan, S.Q. Ran, K.P. Wang, Purification, structural elucidation and anti-inflammatory activity in vitro of polysaccharides from Smilax China L, Int. J. Biol. Macromol. 139 (2019) 233–243, https://doi.org/10.1016/j.ijbiomac.2019.07.209.
[29] Z.Z. Ming, L. Han, M.Y. Bao, H.H. Zhu, S.J. Qiang, S.B. Xue, W.W. Liu, Living bacterial hydrogels for accelerated infected wound healing, Adv. Sci. 8 (24) (2021) 2102545, https://doi.org/10.1002/advs.202102545.
[30] H. Zhang, X.Y. Sun, J. Wang, Y.L. Zhang, M.N. Dong, T. Bu, L.H. Li, Y.N. Liu, L. Wang, Multifunctional injectable hydrogel dressings for effectively accelerating wound healing: enhancing biomineralization strategy, Adv. Funct. Mater. 31 (23) (2021) 2100093, https://doi.org/10.1002/adfm.202100093.
[31] F. Fang, Y.Q. Li, X.Y. Lu, K.Z. Wu, L.Y. Zhou, Y.X. Sun, J.H. Wu, J. Gao, Effect of potential postbiotics derived from food-isolated Lactobacillus on different of human microbiome, LWT–Food Sci. Technol. 182 (2023) 8, https://doi.org/10.1016/j.lwt.2023.114782.
[32] Y.F. Lu, H.S. Li, J. Wang, M.Y. Yao, Y. Peng, T.F. Liu, Z. Li, G.X. Luo, J. Deng, Engineering bacteria-activated multifunctionalized hydrogel for promoting diabetic wound healing, Adv. Funct. Mater. 31 (48) (2021) 2105749, https://doi.org/10.1002/adfm.202105749.
[33] C.X. Cao, Y. Li, C. Wang, N.Q. Zhang, X.Y. Zhu, R.N. Wu, J.R. Wu, Purification, characterization and antitumor activity of an exopolysaccharide produced by Bacillus velezensis SN-1, Int. J. Biol. Macromol. 156 (2020) 354–361, https://doi.org/10.1016/j.ijbiomac.2020.04.024.
[34] H.W. Fan, F. Liu, S.W.A. Bligh, S.S. Shi, S.C. Wang, Structure of a homofructosan from Saussurea costus and anti-complementary activity of its sulfated derivatives, Carbohydr. Polym. 105 (2014) 152–160, https://doi.org/10.1016/j.carbpol.2014.01.084.
[35] F.S. Li, X. Hu, L.Y. Qin, H.S. Li, Y. Yang, X.L. Zhang, J.R. Lu, Y.M. Li, M.T. Bao, Characterization and protective effect against ultraviolet radiation of a novel exopolysaccharide from Bacillus marcorestinctum QDR3-1, Int. J. Biol. Macromol. 221 (2022) 1373–1383, https://doi.org/10.1016/j.ijbiomac.2022.09.114.
[36] X. Wang, M.Y. Huang, F. Yang, H.J. Sun, X.X. Zhou, X.L. Wang, M.L. Zhang, Rapeseed polysaccharides as prebiotics on growth and acidifying activity of probiotics in vitro, Carbohydr. Polym. 125 (2015) 232–240, https://doi.org/10.1016/j.carbpol.2015.02.040.
[37] A.X. Song, Y.H. Mao, K.C. Siu, W.C.S. Tai, J.Y. Wu, Protective effects of exopolysaccharide of a medicinal fungus on probiotic bacteria during cold storage and simulated gastrointestinal conditions, Int. J. Biol. Macromol. 133 (2019) 957–963, https://doi.org/10.1016/j.ijbiomac.2019.04.108.
[38] R. Wang, K. Guo, W.J. Zhang, Y.N. He, K. Yang, Q. Chen, L. Yang, Z.G. Di, J.K. Qiu, P. Lei, Y.A. Gu, Z.S. Luo, X.Q. Xu, Z.Q. Xu, X.H. Feng, S. Li, Z.Y. Yu, H. Xu, Poly-gamma-Glutamic acid microgel-encapsulated probiotics with gastric acid resistance and smart inflammatory factor targeted delivery performance to ameliorate colitis, Adv. Funct. Mater. 32 (26) (2022) 2113034, https://doi.org/10.1002/adfm.202113034.
[39] N. Asadi, H. Pazoki-Toroudi, A.R. Del Bakhshayesh, A. Akbarzadeh, S. Davaran, N. Annabi, Multifunctional hydrogels for wound healing: Special focus on biomacromolecular based hydrogels, Int. J. Biol. Macromol. 170 (2021) 728–750, https://doi.org/10.1016/j.ijbiomac.2020.12.202.
[40] C. Karavasili, K. Tsongas, Andreadis II, E.G. Andriotis, E.T. Papachristou, R. M. Papi, D. Tzetzis, D.G. Fatouros, Physico-mechanical and finite element analysis evaluation of 3D printable alginate-methylcellulose inks for wound healing applications, Carbohydr. Polym. 247 (2020) 10, https://doi.org/10.1016/j.carbpol.2020.116666.
[41] P. Iranmanesh, A. Ehsani, A. Khademi, A. Asefnejad, S. Shahriari, M. Soleimani, M. G. Nejad, S. Saber-Samandari, A. Khandan, Application of 3D bioprinters for dental pulp regeneration and tissue engineering (porous architecture), Transport Porous Media 142 (1–2) (2022) 265–293, https://doi.org/10.1007/s11242-021-01618-x.
[42] D. Guérin, J.C. Vuillemard, M. Subirade, Protection of bifidobacteria encapsulated in polysaccharide-protein gel beads against gastric juice and bile, J. Food Protect. 66 (11) (2003) 2076–2084, https://doi.org/10.4315/0362-028x-66.11.2076.
[43] K. Liu, X.Z. Dong, Y. Wang, X.P. Wu, H.L. Dai, Dopamine-modified chitosan hydrogel for spinal cord injury, Carbohydr. Polym. 298 (2022) 120047, https://doi.org/10.1016/j.carbpol.2022.120047.
[44] A. Zapasnik, B. Sokolowska, M. Bryla, Role of lactic acid bacteria in food preservation and safety, Foods 11 (9) (2022) 1283, https://doi.org/10.3390/foods11091283.
[45] V. Falanga, Wound healing and its impairment in the diabetic foot, Lancet 366 (9498) (2005) 1736–1743, https://doi.org/10.1016/s0140-6736(05)67700-8.
[46] J. Zhang, J. Muri, G. Fitzgerald, T. Gorski, R. Gianni-Barrera, E. Masschelein, G. D'Hulst, P. Gilardoni, G. Turiel, Z. Fan, T.T. Wang, M. Planque, P. Carmeliet, L. Pellerin, C. Wolfrum, S.M. Fendt, A. Banfi, C. Stockmann, I. Soro-Arnaiz, M. Kopf, K. De Bock, Endothelial lactate controls muscle regeneration from ischemia by inducing M2-like macrophage polarization, Cell Metabol. 31 (6) (2020) 1136–1153, https://doi.org/10.1016/j.cmet.2020.05.004.
[47] K. Dietl, K. Renner, K. Dettmer, B. Timischl, K. Eberhart, C. Dorn, C. Hellerbrand, M. Kastenberger, L.A. Kunz-Schughart, P.J. Oefner, R. Andreesen, E. Gottfried, M. P. Kreutz, Lactic acid and acidification inhibit TNF secretion and glycolysis of human monocytes, J. Immunol. 184 (3) (2010) 1200–1209, https://doi.org/10.4049/jimmunol.0902584.
[48] Y.F. Lu, H.S. Li, J. Wang, M.Y. Yao, Y. Peng, T.F. Liu, Z. Li, G.X. Luo, J. Deng, Engineering bacteria-activated multifunctionalized hydrogel for promoting diabetic wound healing, Adv. Funct. Mater. 31 (48) (2021) 13, https://doi.org/10.1002/adfm.202105749.
[49] U.A. Okonkwo, L.A. DiPietro, Diabetes and wound angiogenesis, Int. J. Mol. Sci. 18 (7) (2017) 15, https://doi.org/10.3390/ijms18071419.
[50] Y.N. Qian, Y.J. Zheng, J. Jin, X. Wu, K.J. Xu, M.L. Dai, Q. Niu, H. Zheng, X.J. He, J. L. Shen, Immunoregulation in diabetic wound repair with a photoenhanced glycyrrhizic acid hydrogel scaffold, Adv. Mater. 34 (29) (2022) 15, https://doi.org/10.1002/adma.202200521.
[51] M. Tomic-Canic, J.L. Burgess, K.E. O'Neill, N. Strbo, I. Pastar, Skin microbiota and its interplay with wound healing, Am. J. Clin. Dermatol. 21 (SUPPL 1) (2020) 36–43, https://doi.org/10.1007/s40257-020-00536-w.
[52] P. Chen, G.W. He, J.R. Qian, Y. Zhan, R. Xiao, Potential role of the skin microbiota in Inflammatory skin diseases, J. Cosmet. Dermatol. 20 (2) (2021) 400–409, https://doi.org/10.1111/jocd.13538.
[53] M. Assarsson, A. Duvetorp, O. Dienus, J. Söderman, O. Seifert, Significant changes in the skin microbiome in patients with chronic plaque psoriasis after treatment with narrowband ultraviolet B, Acta Derm. Venereol. 98 (4) (2018) 428–436, https://doi.org/10.2340/00015555-2859.
[54] H. Chen, Q. Zhao, Q. Zhong, C. Duan, J. Krutmann, J. Wang, J. Xia, Skin microbiome, metabolome and skin phenome, from the perspectives of skin as an ecosystem, Phenomics (Cham, Switzerland) 2 (6) (2022) 363–382, https://doi.org/10.1007/s43657-022-00073-y.
[55] S.M. Ali, G. Yosipovitch, Skin pH: from basic science to basic skin Care, Acta Derm. Venereol. 93 (3) (2013) 261–267, https://doi.org/10.2340/00015555-1531.
[56] T. Maheswary, A.A. Nurul, M.B. Fauzi, The insights of microbes' roles in wound healing: a comprehensive review, Pharmaceutics 13 (7) (2021) 22, https://doi.org/10.3390/pharmaceutics13070981.